Diruthenium Complexes | *Hot Paper*

The Indigo Isomer Epindolidione as a Redox-Active Bridging Ligand for Diruthenium Complexes

Maya Kumari,[a] Sudip Kumar Bera,[a] Svenja Blickle,[b] Wolfgang Kaim,*[b] and Goutam Kumar Lahiri*[a]

Abstract: Epindolidione (H_2L), a heteroatom-modified analogue of tetracene and a structural isomer of indigo, forms dinuclear complexes with $[RuX_2]^{2+}$, X = bpy (2,2′-bipyridine, $[\mathbf{1}]^{2+}$) or pap (2-phenylazopyridine, $[\mathbf{2}]^{2+}$), in its doubly deprotonated bridging form μ-L^{2-}. The dications in compounds *meso*-$[\mathbf{1}](ClO_4)_2$ and *meso*-$[\mathbf{2}](ClO_4)_2$, $[X_2Ru(\mu\text{-}L)RuX_2](ClO_4)_2$, contain five-membered chelate rings N-C–C-O-Ru^{II} with π bridged metals at an intramolecular distance of 7.19 Å. Stepwise reversible oxidation and reduction is mainly ligand centered (oxidation: L^{2-}; reduction: X), as deduced from EPR of one-electron oxidized and reduced intermediates and from UV/Vis/NIR spectroelectrochemistry, supported by TD-DFT calculation results. The results for $[\mathbf{1}](ClO_4)_2$ and $[\mathbf{2}](ClO_4)_2$ are qualitatively similar to the ones observed with the deprotonated indigo-bridged isomers with their six-membered chelate ring structures, confirming the suitability of both π systems for molecular electronics applications, low-energy absorptions, and multiple electron transfers.

Introduction

The presence of a π conjugated system and of N and O heteroatoms with potential chelating functionality have made indigo an intriguing ligand[1,2] for redox-active coordination compounds,[3] including dinuclear complexes.[2] A structural isomer of indigo is epindolidione = 5,11-dihydroquinolino[3,2-*b*]quinoline-6,12-dione = H_2L (Scheme 1),[4] which can also be viewed as a modified tetracene[5] ring system. Although computational studies[6] and the formation of transition-metal complexes of H_2L/L^{2-} have been described earlier,[7] more recent interest has been given to H_2L as a component in molecular electronics,[8–13] especially regarding organic field-effect transistors (OFETs).

In following up previous work on the coordination chemistry of redox-active ruthenium with indigo-type ligands,[2] we are now presenting two diruthenium complexes $[\mathbf{1}](ClO_4)_2$ and $[\mathbf{2}](ClO_4)_2$ with doubly deprotonated epindolidione (Scheme 2). Advancing earlier work,[7] we can provide structural information from X-ray diffraction, electrochemical potentials for multiple electron transfer, and spectroelectrochemical identification (EPR, UV/Vis/NIR) of intermediates.[2,14]

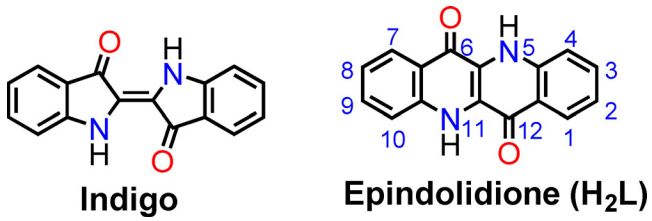

Scheme 1. Structural isomers of indigo and epindolidione.

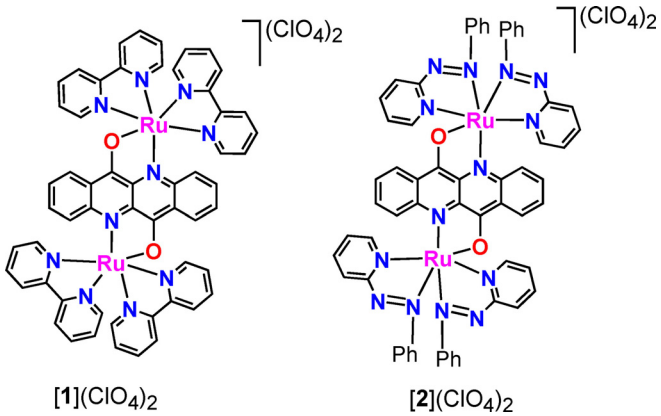

Scheme 2. The two diruthenium complexes $[\mathbf{1}](ClO_4)_2$ and $[\mathbf{2}](ClO_4)_2$ with doubly deprotonated epindolidione presented in this work.

[a] *M. Kumari, S. K. Bera, Prof. Dr. G. K. Lahiri*
Department of Chemistry, Indian Institute of Technology Bombay
Powai, Mumbai 400076 (India)
E-mail: lahiri@chem.iitb.ac.in
[b] *S. Blickle, Prof. Dr. W. Kaim*
Institut für Anorganische Chemie, Universität Stuttgart
Pfaffenwaldring 55, 70550 Stuttgart (Germany)
E-mail: kaim@iac.uni-stuttgart.de
Supporting information and the ORCID identification number(s) for the author(s) of this article can be found under: https://doi.org/10.1002/chem.202004747.

Results and Discussion

Synthesis and characterization

The diruthenium complexes $[(bpy)_2Ru^{II}(\mu\text{-}L)Ru^{II}(bpy)_2](ClO_4)_2$ ([**1**](ClO$_4$)$_2$) and $[(pap)_2Ru^{II}(\mu\text{-}L)\ Ru^{II}(pap)_2](ClO_4)_2$ ([**2**](ClO$_4$)$_2$) bridged by doubly deprotonated epindolidione were obtained from ethanolic solution of H_2L and in situ generated metal precursors *cis*-$[Ru(bpy)_2(C_2H_5OH)_2]^{2+}$ (bpy = 2,2′-bipyridine) or *ctc*-$[Ru(pap)_2(C_2H_5OH)_2]^{2+}$ (pap = 2-phenylazopyridine, *ctc* = *cis*–*trans*–*cis* with respect to C_2H_5OH, pyridine, and azo nitrogens of two pap units), respectively, in the presence of NEt_3 base. The complexes were purified by column chromatography (see the Experimental Section). Thin layer chromatographic (TLC) experiments further established the exclusive formation of one diastereomeric form for both [**1**](ClO$_4$)$_2$ and [**2**](ClO$_4$)$_2$, identified as the *meso* isomer in both cases (see below).

The diamagnetic and 1:2-conducting compounds [**1**](ClO$_4$)$_2$ and [**2**](ClO$_4$)$_2$ were characterized by C,H,N analysis, mass spectrometry, and ^{1}H NMR spectral features (Experimental Section and Figures S1–S3 in the Supporting Information). The ^{1}H NMR spectra of [**1**](ClO$_4$)$_2$ and [**2**](ClO$_4$)$_2$ exhibit partially overlapping proton resonances in the chemical shift range $\delta = 9.0$–6.0 ppm.

Crystal structures

The molecular structures of the dications in the crystals of [**1**](ClO$_4$)$_2$ and [**2**](ClO$_4$)$_2$ were determined by X-ray crystallography (Figure 1, Table 1). The bpy-containing compound crystallizes with two independent molecules (Figure S4 in the Supporting Information). Figure 1 shows perspective views with

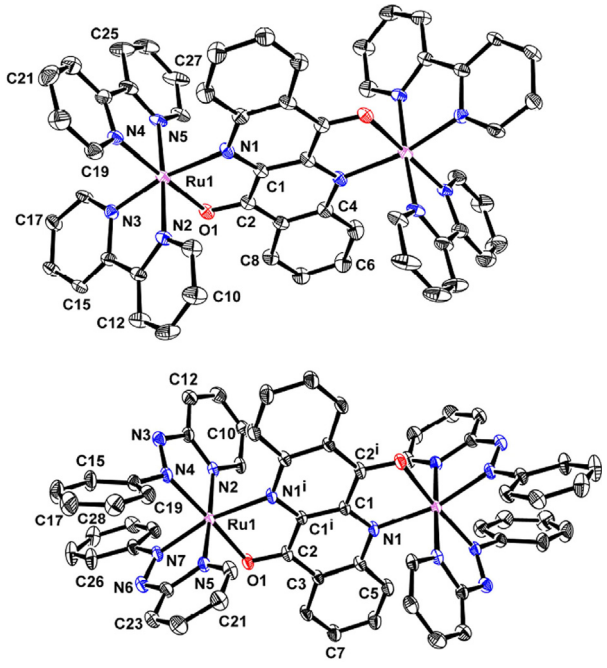

Figure 1. Perspective views of the cations of (a) [**1**](ClO$_4$)$_2$ (molecule A) and (b) [**2**](ClO$_4$)$_2$. Ellipsoids are drawn at the 30% probability level. Hydrogen atoms and counter anions are omitted for clarity.

Table 1. Selected crystallographic parameters.

Complex	[**1**](ClO$_4$)$_2$	[**2**](ClO$_4$)$_2$
empirical formula	$C_{56}H_{40}Cl_2N_{10}O_{10}Ru_2$	$C_{60}H_{44}Cl_2N_{14}O_{10}Ru_2$
formula weight	1286.02	1394.13
crystal system	triclinic	monoclinic
space group	$P\bar{1}$	$C12/c1$
a [Å]	12.1695(3)	19.4787(10)
b [Å]	15.1125(4)	21.1488(9)
c [Å]	16.4956(3)	14.6286(8)
α [°]	77.081(2)	90
β [°]	79.430(2)	88.820(5)
γ [°]	78.802(2)	90
V [Å^3]	2869.37(12)	6025.0(5)
Z	2	4
μ [mm^{-1}]	0.685	0.661
T [K]	150(2)	150(2)
D_{calcd} [g cm^{-3}]	1.488	1.537
F (000)	1296	2816
θ range [°]	1.703 to 24.999	1.926 to 32.230
data/restraints/parameters	10 108/0/721	9304/0/397
$R1$, $wR2$ [$I > 2\sigma(I)$]	0.0946, 0.2507	0.0669, 0.1778
$R1$, $wR2$ (all data)	0.1105, 0.2700	0.1008, 0.1973
GOF on F^2	1.065	1.112
largest diff. peak/hole [e Å^{-3}]	3.677/−1.155	1.744/−1.281

atomic numbering and Table 2 presents significant distances. More complete lists of bond lengths and angles are given in comparison to DFT-computed and well-reproduced values in Tables S1 and S2 (in the Supporting Information).

Table 2. Selected experimental bond lengths and distances [Å] for [**1**](ClO$_4$)$_2$ and [**2**](ClO$_4$)$_2$.

Bond	[**1**](ClO$_4$)$_2$[a]	[**2**](ClO$_4$)$_2$
Ru1–N1	2.127(6)	2.127(3)
Ru1–N2	2.046(7)	2.059(3)
Ru1–N3	2.027(7)	–
Ru1–N4	2.042(6)	1.999(3)
Ru1–N5	2.020(6)	2.036(3)
Ru1–N7	–	2.046(3)
Ru1–O1	2.066(5)	2.092(2)
C1–N1	1.364(10)	1.355(4)
N3–N4	–	1.285(4)
N6–N7	–	1.290(4)
C2–O1	1.292(9)	1.290(4)
C1–C2	1.419(11)	1.407(6)
Ru1···Ru2	7.185	7.196

[a] Molecule A.

Both dications $[\mathbf{1}]^{2+}$ and $[\mathbf{2}]^{2+}$ were found as *meso* diastereoisomers.[15] They exhibit intramolecular metal–metal bond lengths of about 7.19 Å. The bond Ru–N1 from the donating Ru^{II} metal to the partially charged N donor center of L^{2-} is long (2.127 Å) in comparison to the shorter Ru–N distances (≈2.03 Å) to the neutral π-accepting peripheral ligands bpy and pap. Characteristically, the N–N (azo) bond in pap co-ligands of $[\mathbf{2}]^{2+}$ is about 1.29 Å, suggesting dπ(Ru^{II}) to π*(N=N) charge transfer (back boding) in the ground state.[16,17] The Ru–N1 bond in the five-membered chelate rings Ru1-N1-C1-

C2-O1 is also longer than Ru–O1 with the less basic oxygen donor atom.

Electrochemistry

Both compounds [**1**]$(ClO_4)_2$ and [**2**]$(ClO_4)_2$ exhibit two waves, O1 and O2, for reversible oxidation, separated by about 0.4 V, and several waves for cathodic reduction (Figure 2, Table 3, and Figure S5 in the Supporting Information). All corresponding features lie at more positive potentials for the pap-containing system with the stronger π-acceptor co-ligand. It is thus likely that the two facile reduction processes R1 and R2 for [**2**]$(ClO_4)_2$ are attributable to electron uptake by pap ligands on opposite sides of the dinuclear molecule. On the other hand, the crowding of reductions R1–R5 at negative potentials for [**1**]$(ClO_4)_2$ suggests bpy-based processes with little intramolecular interaction. The number of electrons associated with the reversible redox processes in Figure 2 was evaluated by spectroelectrochemistry (see below).

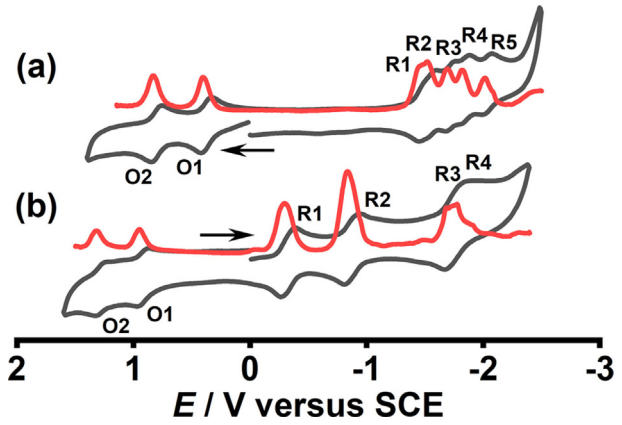

Figure 2. Cyclic (black) and differential pulse (red) voltammograms of (glassy carbon working electrode): (a) [**1**]$(ClO_4)_2$ and (b) [**2**]$(ClO_4)_2$ in CH_3CN/0.1 M Et_4NClO_4.

Oxidation can be attributed either to the metals, leading to mixed-valent $Ru^{III}Ru^{II}$ intermediates,[18,19] or to the central π-conjugated ligand L^{2-} with its donor character, leading to a bridging radical anion.[20,21] EPR spectroelectrochemistry with determination of the *g* factor anisotropy is suitable to answer this question because the participation of heavy elements such as ruthenium with their high spin-orbit coupling contributions strongly affects the behavior of *g*.[22,23]

EPR spectroscopy

Starting from the dicationic complexes $[\mathbf{1}]^{2+}$ and $[\mathbf{2}]^{2+}$, the in situ electrolysis yields one-electron oxidized and reduced paramagnetic species, the EPR spectra of which are shown in Figures 3–6 together with computer simulations. The data obtained in fluid and frozen solutions are listed in Table 4, whereas calculated relevant spin densities are listed in Table 5 and illustrated in Figures 7 and 8.

The EPR spectra reveal only small deviations of *g* from the *g* (electron) value of 2.0023 and thus ligand-based spin is assumed in all instances, albeit with characteristic modifications. A relatively large *g* anisotropy $g_1-g_3=0.672$ in the low-temperature spectrum is noted for $[\mathbf{1}]^{3+}$, supported by notable spin densities of 0.151 on each of the metals. This result suggests significant contributions from the $Ru^{2.5}(\mu\text{-}L^{2-})Ru^{2.5}$ formulation with metal-centered spin in addition to the dominant $Ru^{II}(\mu\text{-}L^{\cdot-})Ru^{II}$ contribution.[22,23] The latter is much more favored for $[\mathbf{2}]^{3+}$ where the strong π-acceptor pap[16,17] stabilizes the ruthenium(II) states. Accordingly, spin densities are smaller on the

Table 3. Electrochemical data.[a]

Complex	$E_{1/2}$ [V] (ΔE_p [mV])[b]						
	O2	O1	R1	R2	R3	R4	R5
[**1**]$(ClO_4)_2$	0.80(80)	0.38(100)	−1.50(100)	−1.57(70)	−1.72(70)	−1.85(60)	−2.05(80)
[**2**]$(ClO_4)_2$	1.28(70)	0.91(100)	−0.33(120)	−0.87(140)	−1.68(160)	−1.77(190)	–

[a] From cyclic voltammetry in CH_3CN/0.1 M Et_4NClO_4 at 100 mVs^{-1}. [b] Potentials in V versus saturated calomel electrode (SCE); peak potential differences ΔE_p [mV] in parentheses.

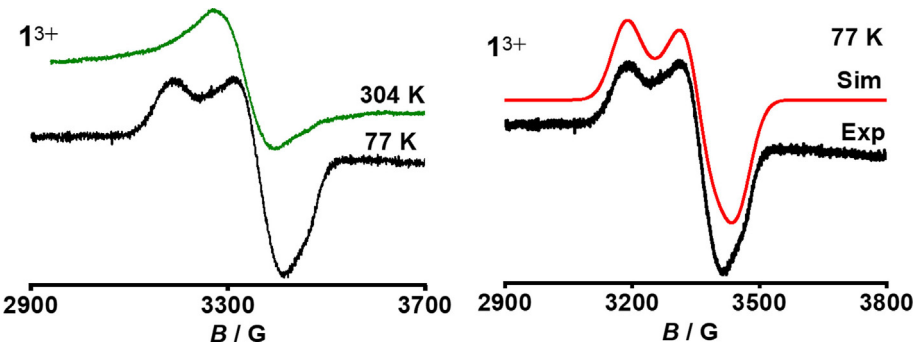

Figure 3. EPR spectra of in situ generated $[\mathbf{1}]^{3+}$ in 0.1 M CH_2Cl_2/Bu_4NPF_6.

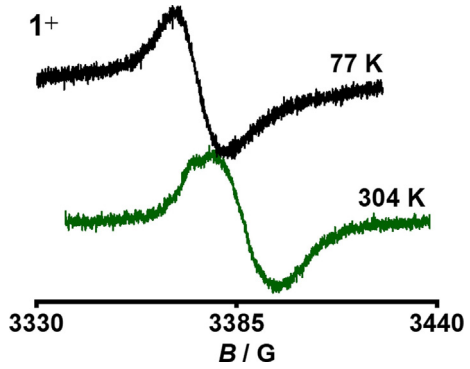

Figure 4. EPR spectra of in situ generated $[\mathbf{1}]^{+}$ in 0.1 M CH_2Cl_2/Bu_4NPF_6.

Table 4. EPR data.[a]

Complex ion	T [K]	g_{iso}	g_1	g_2	g_3	$\langle g \rangle$[b]	Δg[c]
$[\mathbf{1}]^{3+}$	300	2.028					
	77		2.121	2.010	1.956	2.030	0.672
$[\mathbf{1}]^{+}$	300	2.0027					
	77		2.006	1.998	1.998	2.0005	0.008
$[\mathbf{2}]^{3+}$	300	2.003					
	77		2.036	1.998	1.998	2.010	0.038
$[\mathbf{2}]^{+}$	300	1.998					
	77		2.016	1.997	1.997	2.003	0.019

[a] From spectroelectrochemistry in CH_2Cl_2/0.1 M Bu_4NPF_6. [b] $\langle g \rangle = \{(1/3)(g_1^2+g_2^2+g_3^2)\}^{1/2}$. [c] $\Delta g = g_1 - g_3$.

metals (0.101, Table 5) and the g anisotropy Δg is diminished (Table 4).

The one-electron reduced forms show very little metal contribution to the spin distribution, and the g variations with $\Delta g < 0.02$ suggest mainly the π-accepting co-ligands, bpy or pap, as sites for electron uptake.

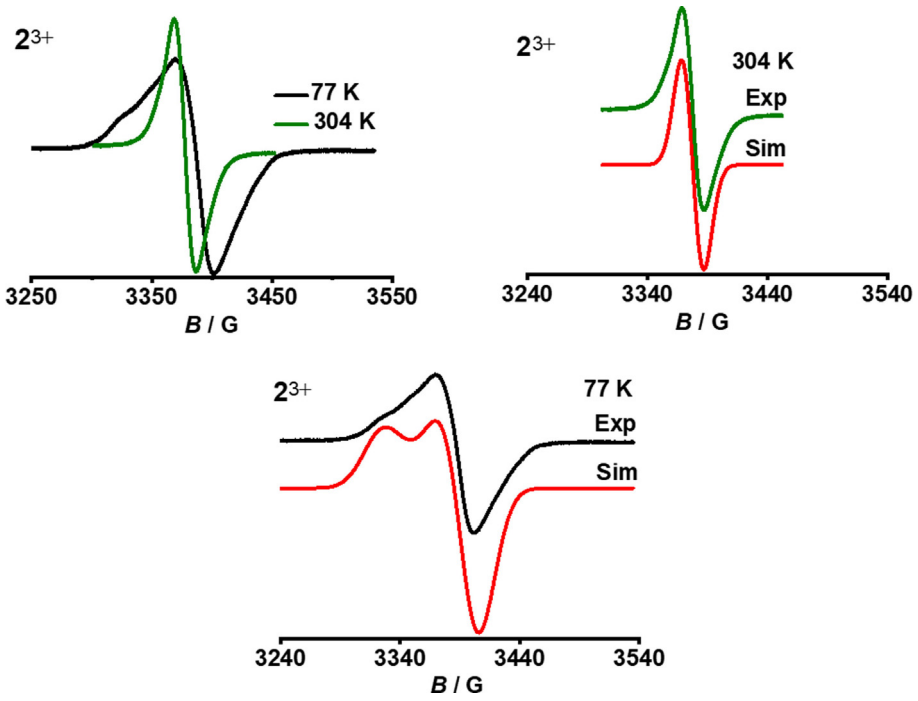

Figure 5. EPR spectra of in situ generated $[\mathbf{2}]^{3+}$ in 0.1 M CH_2Cl_2/Bu_4NPF_6.

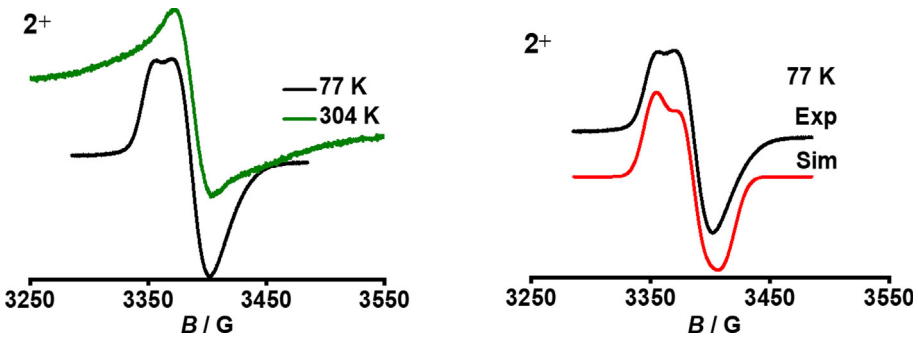

Figure 6. EPR spectra of in situ generated $[\mathbf{2}]^{+}$ in 0.1 M CH_2Cl_2/Bu_4NPF_6.

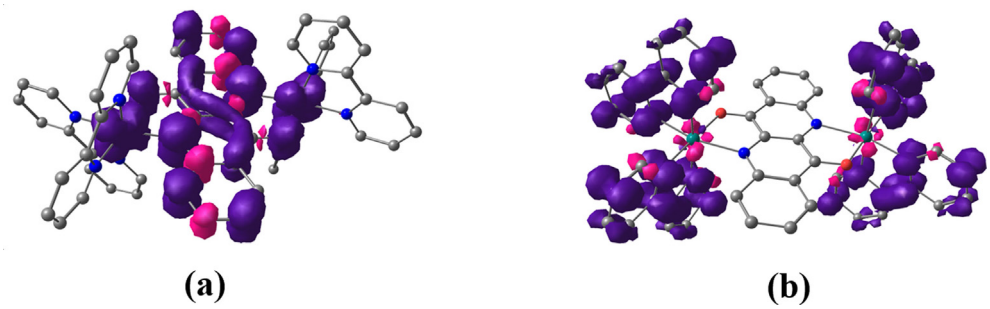

Figure 7. Spin density representations of (a) $\mathbf{1}^{3+}$ ($S=1/2$) and (b) $\mathbf{1}^{+}$ ($S=1/2$).

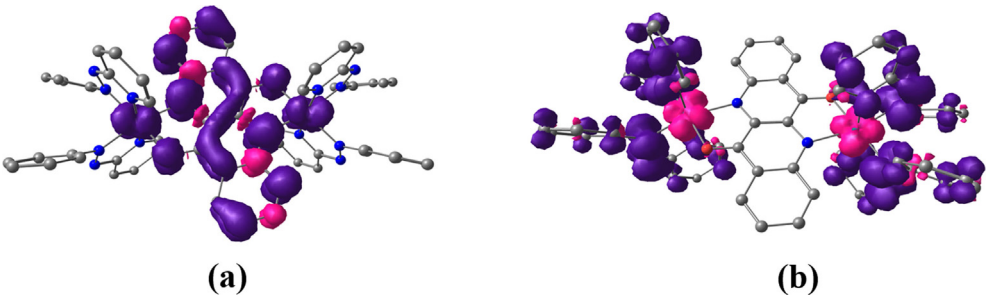

Figure 8. Spin density representations of (a) $\mathbf{2}^{3+}$ ($S=1/2$) and (b) $\mathbf{2}^{+}$ ($S=1/2$).

Table 5. DFT-calculated (UB3LYP/LanL2DZ/6-31G*) Mulliken spin densities for the paramagnetic forms of $\mathbf{1}^n$ and $\mathbf{2}^n$.

Complex	Ru1/Ru2	L	bpy or pap
$\mathbf{1}^{3+}$ ($S=1/2$)	0.151/0.151	0.710	−0.012
$\mathbf{1}^{+}$ ($S=1/2$)	−0.014/−0.014	0.012	0.984
$\mathbf{2}^{3+}$ ($S=1/2$)	0.101/0.101	0.815	−0.017
$\mathbf{2}^{+}$ ($S=1/2$)	−0.085/−0.085	0.000	1.170
$\mathbf{2}^{0}$ ($S=1$)	−0.184/−0.184	0.010	2.358
$\mathbf{2}^{-}$ ($S=3/2$)	0.057/0.057	0.010	2.876

UV/Vis/NIR spectroelectrochemistry

Spectroelectrochemistry in the UV/Vis/NIR region could be performed for various accessible charge states (Figures 9 and 10) by using an OTTLE cell.[14,24] Table 6 summarizes the experimental data and Table S3 (in the Supporting Information) lists the results from TD-DFT calculations. Further computational results are collected in Tables S4–S16 (in the Supporting Information).

An overall inspection of spectral information and computational results reveals that the main low-energy absorptions of the dicationic starting compounds in the visible region involve metal-to-ligand charge transfer (MLCT) transitions to the peripheral π-acceptors (bpy or pap) and transitions originating from the bridging donor ligand L^{2-}.

On oxidation to the trications, intense bands ($\varepsilon > 6000\ M^{-1}cm^{-1}$) emerge in the near infrared ($\lambda_{max} > 1000$ nm), which show mixed character according to the resonance formulation $[X_2Ru^{II}(\mu\text{-}L^{\cdot-})Ru^{II}X_2]^{3+} \leftrightarrow [X_2Ru^{2.5}(\mu\text{-}L^{2-})Ru^{2.5}X_2]^{3+}$ with options for metal-to-metal charge transfer (MMCT) and ligand-to-ligand charge transfer (LLCT) transitions.[22] Further oxidation to the tetracationic forms results in a slight hypsochromic shift to about 960 nm and an intensity increase ($\varepsilon > 20\,000\ M^{-1}cm^{-1}$) of the near infrared band, attributed to MLCT transitions to π* orbitals of the oxidized neutral bridge L^0.

One-electron reduction of the starting materials to monocations yields little changed spectra in agreement with the first and then successive further electron addition to the peripheral co-ligands bpy or pap in $[\mathbf{1}]^n$ or $[\mathbf{2}]^n$, respectively. Reduced bpy and pap are known to exhibit low-energy but less intense intra-ligand absorptions.[16,17,25]

Conclusion

In doubly deprotonated form, the constitutional isomers derived from epindolidione and indigo[2] can both form bridged diruthenium complexes with predominantly ligand-based electron transfer. In addition to the electronic variation, the coordination behavior is different owing to the formation of two five-membered chelate rings with L^{2-} in contrast to two six-membered chelate rings with deprotonated indigo in its *trans* configuration (Scheme 3).[2]

Structural investigation of the complexes $[X_2Ru(\mu\text{-}L)RuX_2](ClO_4)_2$, X = bpy (**1**) or pap (**2**), shows that doubly deprotonated epindolidione L^{2-} can act as a bis-chelating ligand, as assumed by Schmidt and Beck.[7] The π-conjugated bridging function of L^{2-}, a structural isomer of doubly deprotonated indigo,[2,26] and the intramolecular Ru–Ru distance of about 7.19 Å suggest a potential metal–metal mediating function of L^n, however, spectroelectrochemical measurements (EPR, UV/Vis/NIR) for several reversible oxidation and reduction processes point to predominantly ligand-based electron transfer pro-

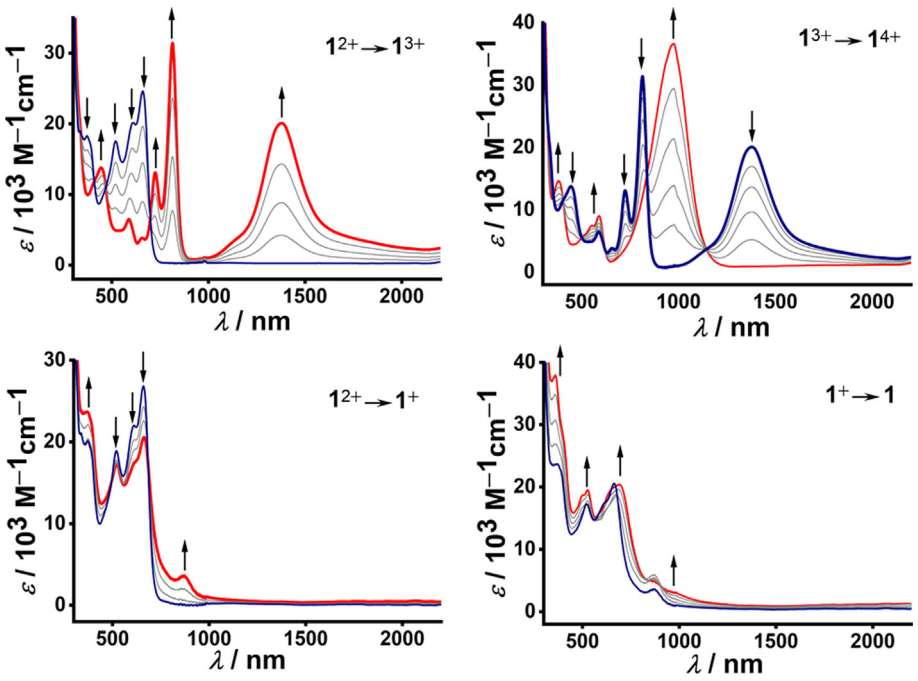

Figure 9. UV/Vis/NIR spectroelectrochemical response of $\mathbf{1}^n$ in M CH_3CN/0.1 M Bu_4NPF_6.

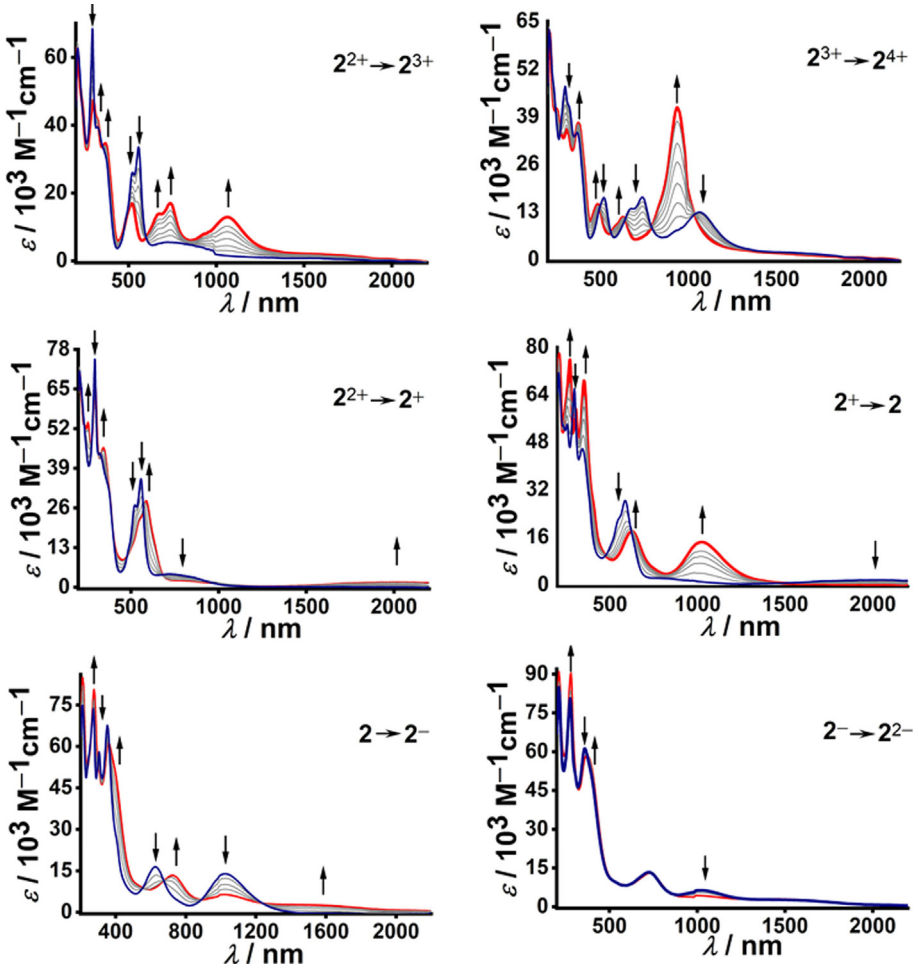

Figure 10. UV/Vis/NIR spectroelectrochemical response of $\mathbf{2}^n$ in M CH_3CN/0.1 M Bu_4NPF_6.

Table 6. Electronic spectral data.

Complex	λ [nm] (ε [$M^{-1}cm^{-1}$])
$\mathbf{1}^{4+}$	977 (36600), 590 (9000), 552sh (7500), 383 (14600)
$\mathbf{1}^{3+}$	1380 (20100), 814 (31400), 725 (13100), 446 (13800)
$\mathbf{1}^{2+}$	660 (24600), 608 (20200), 520 (17500), 372 (18200)
$\mathbf{1}^{+}$	871 (3600), 664 (20600), 608sh (17200), 522 (17300), 371 (23700)
$\mathbf{2}^{4+}$	940 (20600), 627 (5800), 586sh (4600), 485 (7500), 374 (18600), 309 (17700)
$\mathbf{2}^{3+}$	1060 (6400), 736 (8500), 670sh (6900), 520 (8400), 368 (17300), 326sh (20500), 299 (23600)
$\mathbf{2}^{2+}$	740 (2700), 557 (16800), 523 (13000), 370sh (15400), 320 (19800), 295 (34200)
$\mathbf{2}^{+}$	2000 (800), 588 (14100), 544sh (10700), 344 (22900), 297 (32900), 256 (27000)
$\mathbf{2}^{0}$	1022 (7200), 625 (9000), 410sh (12800), 353 (34300), 305 (29600), 272 (37900)
$\mathbf{2}^{-}$	1550 (1300), 1020(3200), 727 (6700), 400sh (25100), 360 (30600), 275 (40000)
$\mathbf{2}^{2-}$	1550 (1300), 730 (6700), 380 (29100), 280 (45200)

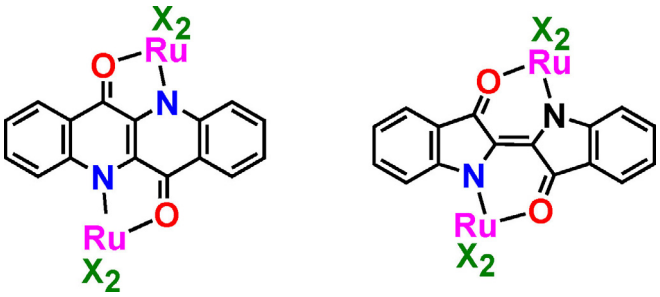

Scheme 3. The structures with two five-membered chelate rings with L^{2-} and two six-membered chelate rings with deprotonated indigo in its *trans* configuration.

cesses in the accessible region, similarly to the behavior of indigo-bridged analogs.[2,26] Scheme 4 illustrates the redox series as deduced from structure determination, spectroelectrochemistry, and DFT calculations.

Oxidation involves the π-donating bridge with minor metal contributions whereas reductions occur at the peripheral π acceptors bpy or pap, the latter exhibiting stronger effects.

The complexes $[X_2Ru(\mu\text{-}L)RuX_2]^n$ do not only exhibit ligand-centered spin on oxidation and reduction (EPR, DFT), they also

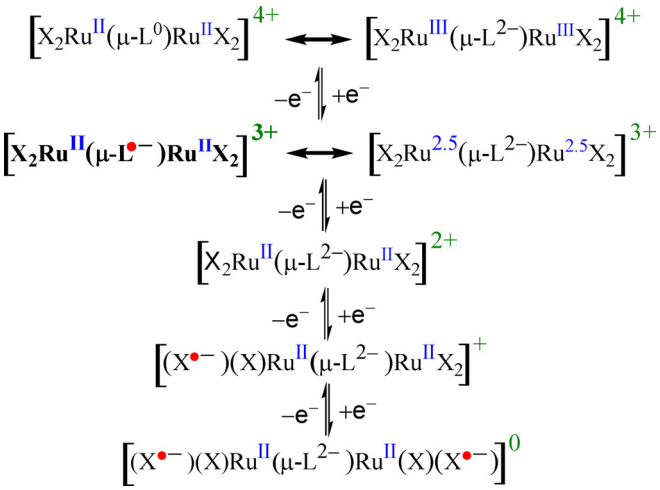

Scheme 4. Redox series with oxidation state assignments. Main contribution for (3+) form indicated by boldface.

reveal rather intense long-wavelength absorptions in the near infrared (NIR)[27] for the one-electron oxidized intermediates ($\lambda_{max} > 1000$ nm) and especially for the two-electron oxidized species ($\lambda_{max} \approx 960$ nm). Such patterns, which may be useful in information technology,[27] have been observed before[21] for ruthenium complexes with tunable electron-donating non-innocent bridging ligands.

Apparently, the L^{n-} system has considerable potential with respect to various physical properties,[8–13] including metal coordination, low-energy electronic absorptions, and radical stabilization through optimum spin distribution. It thus constitutes a viable alternative to the isomeric indigo π system, sharing a number of common features.

Experimental Section

Materials

The ligand precursor H_2L[4] and the starting complexes *cis*-[Ru(bpy)$_2$Cl$_2$][28a] and *ctc*-[Ru(pap)$_2$Cl$_2$][28b] were synthesized according to the literature procedures. Other chemicals and solvents were of reagent grade and used as received. For spectroscopic and electrochemical studies, HPLC grade solvents were used.

Physical measurements

The electrical conductivity was checked by using an autoranging conductivity meter (Toshcon Industries, India). The EPR measurements were made in a two-electrode capillary tube[20] with an X-band (9.5 GHz) Bruker system ESP300 spectrometer. Cyclic voltammetric and differential pulse voltammetric measurements of the complexes were done by using a PAR model 273A electrochemistry system. A glassy carbon working electrode, platinum wire auxiliary electrode, and a saturated calomel reference electrode (SCE) were used in a standard three-electrode configuration with tetraethylammonium perchlorate (TEAP) as the supporting electrolyte (substrate concentration $\approx 10^{-3}$ M; standard scan rate 100 mVs^{-1}). UV/Vis/NIR spectroelectrochemical studies were performed in CH_3CN/0.1 M Bu_4NPF_6 at 298 K by using an optically transparent thin-layer electrode (OTTLE) cell[24] mounted in the sample compartment of a J&M TIDAS spectrophotometer. All spectroelectrochemical experiments were carried out under a dinitrogen atmosphere. The half-wave potential $E_{1/2}$ was set equal to $0.5(E_{pa}+E_{pc})$, where E_{pa} and E_{pc} are anodic and cathodic cyclic voltammetry peak potentials, respectively. ^{1}H NMR spectra were recorded with a Bruker Avance III

500 MHz spectrometer. The elemental analyses were performed with a Thermo Finnigan (FLASH EA 1112 series) microanalyzer. Electrospray mass spectra (ESI-MS) were recorded with a Bruker Maxis Impact instrument (282001.00081).

Preparation of complexes

Synthesis of $[(bpy)_2Ru(\mu\text{-}L)Ru(bpy)_2](ClO_4)_2$ [1](ClO$_4$)$_2$: An amount of *cis*-Ru(bpy)$_2$Cl$_2$ (100 mg, 0.21 mmol) and AgClO$_4$ (93 mg, 0.45 mmol) were suspended in EtOH (30 mL) and heated to reflux for 2 h. The precipitated AgCl was filtered through a sintered Gooch crucible. The filtrate was added to a preheated ethanolic solution of H_2L (25 mg, 0.10 mmol) and Et_3N (22 mg, 0.21 mmol) and the mixture was heated to reflux for 6 h under dinitrogen atmosphere. The residue obtained on removal of the solvent was moistened by a few drops of CH_3CN and a saturated aqueous solution of $NaClO_4$ was added and kept overnight at 273 K. The solid mass was filtered off, washed with chilled water to remove excess $NaClO_4$, and dried over P_4O_{10}. The dark-blue product [**1**](ClO$_4$)$_2$ was purified on a neutral alumina column by using a CH_2Cl_2/CH_3CN (4:1) solvent mixture as eluent.

[1](ClO$_4$)$_2$: Yield, 52 mg (78%); ESI-MS (+) in CH_3CN, *m/z* calcd for {[**1**−ClO$_4$}$^+$]): 1187.15; found: 1187.13; ^{1}H NMR (500 MHz, $(CD_3)_2SO$): $\delta = 8.83$ (d, 1H); 8.80–8.60 (m, 7H), 8.49 (d, 1H), 8.18–8.08 (m, 3H), 8.07–7.95 (m, 11H), 7.92 (d, 1H), 7.64–7.56 (m, 3H), 7.48–7.32 (m, 6H), 7.24 (t, 1H), 7.03–6.93 (m, 4H), 6.56–6.49 (m, 1H), 6.45–6.36 ppm (m, 1H); molar conductivity (CH_3CN): $\Lambda_M = 232\ \Omega^{-1}\,cm^2\,M^{-1}$; elemental analysis calcd (%) for $C_{56}H_{40}Cl_2N_{10}O_{10}Ru_2$: C 52.3, H 3.14, N 10.89; found: C 52.45, H 3.37, N 10.79.

Synthesis of $[(pap)_2Ru(\mu\text{-}L)Ru(pap)_2](ClO_4)_2$, [2](ClO$_4$)$_2$: A mixture of Ru(pap)$_2Cl_2$ (100 mg, 0.19 mmol) and AgClO$_4$ (83 mg, 0.40 mmol) in EtOH (40 mL) was heated to reflux for 2 h and the precipitated AgCl was filtered off through a sintered Gooch crucible. The filtrate was added to a preheated ethanolic solution (20 mL) of the ligand (H_2L, 25 mg, 0.095 mmol) and Et_3N (20 mg, 0.20 mmol) and heated at reflux under dinitrogen atmosphere for 8 h. The solvent was removed under reduced pressure and the residue was moistened with a few drops of CH_3CN and a saturated aqueous solution of $NaClO_4$ was added. This was then allowed to cool overnight at 273 K. The precipitate was filtered off and washed thoroughly with chilled water to remove excess $NaClO_4$. It was then dried over P_4O_{10} and the dark-purple product [**2**](ClO$_4$)$_2$ was purified on a neutral alumina column using a CH_2Cl_2/CH_3CN (3:1) solvent mixture as eluent.

[2](ClO$_4$)$_2$: Yield, 40 mg (61%); ESI-MS (+) in CH_3CN, *m/z* calcd for {[**2**-ClO$_4$}$^+$]): 1295.14; found: 1295.13; ^{1}H NMR (500 MHz, $(CD_3)_2SO$): $\delta = 8.76$ (d, 1H), 8.57 (d, 1H), 8.46 (t, 2H), 8.42–8.35 (m, 3H), 8.29 (t, 3H), 8.18 (d, 1H), 8.13–8.06 (m, 2H), 8.03 (d, 2H), 7.99 (d, 1H), 7.95 (t, 1H), 7.90 (t, 2H), 7.68 (t, 2H), 7.51–7.34 (m, 8H), 7.25–7.18 (m, 7H), 7.11 (d, 2H), 7.01 (d, 3H), 6.92 (d, 2H), 6.86 ppm (d, 1H); molar conductivity (CH_3CN): $\Lambda_M = 210\ \Omega^{-1}\,cm^2\,M^{-1}$; elemental analysis calcd (%) for $C_{60}H_{44}Cl_2N_{14}O_{10}Ru_2$: C 51.69, H 3.18, N 14.07; found: C 51.40, H 3.25, N 14.39.

***Caution*!** Perchlorate salts are explosive and should be handled with care.

Crystallography

Single crystals of [**1**](ClO$_4$)$_2$ and [**2**](ClO$_4$)$_2$ were grown by slow evaporation of their 1:1 CH_2Cl_2/CH_3OH solutions. X-ray diffraction data were collected by using a Rigaku Saturn-724+ CCD single-crystal diffractometer using $Mo_{K\alpha}$ radiation at 150(2) K. The data collection was evaluated by using the CrystalClear-SM Expert software. The data were collected by the standard ω-scan technique. The structure was solved by direct methods using SHELXT-2015 and refined by full-matrix least-squares with SHELXL-2017, refining on F^2.[29] All data were corrected for Lorentz and polarization effects and all non-hydrogen atoms were refined anisotropically. The remaining hydrogen atoms were placed in geometrically constrained positions and refined with isotropic temperature factors, generally 1.2 U_{eq} of their parent atoms. Hydrogen atoms were included in the refinement process as per the riding model. SQUEEZE was applied for disordered unidentified solvent molecules in the crystals of [**2**](ClO$_4$)$_2$ using the PLATON[30] program package.

Deposition numbers 2038210 and 2038274 (for [**1**](ClO$_4$)$_2$ and [**2**](ClO$_4$)$_2$, respectively) contain the supplementary crystallographic data for this paper. These data are provided free of charge by the joint Cambridge Crystallographic Data Centre and Fachinformationszentrum Karlsruhe Access Structures service www.ccdc.cam.ac.uk/structures.

Computational details

Full geometry optimizations were carried out by using the density functional theory method at the (U)B3LYP level for $\mathbf{1}^n$ ($n = +3, +1, 0$), $\mathbf{2}^n$ ($n = +3, +1, 0, -1$), and (R)B3LYP for $\mathbf{1}^n$ ($n = +4, +2$), $\mathbf{2}^n$ ($n = +4, +2, -2$).[31] All elements except ruthenium were assigned the 6-31G(d) basis set. The LanL2DZ basis set with effective core potential was employed for the ruthenium atom.[32] All calculations were performed with the Gaussian09 program package.[33] Vertical electronic excitations based on (U)B3LYP optimized geometries were computed by using the time-dependent density functional theory (TD-DFT) formalism[34] in acetonitrile using the conductor-like polarizable continuum model (CPCM).[35] Chemissian 1.7[36] was used to calculate the fractional contributions of various groups to each molecular orbital. All calculated structures were visualized with ChemCraft.[37]

Acknowledgments

Financial support received from Science and Engineering Research Board (SERB, Department of Science and Technology), J. C. Bose Fellowship (G.K.L., SERB), Council of Scientific and Industrial Research (fellowship to M.K.), University Grant Commission (fellowship to S.K.B), New Delhi, India, and the Land Baden-Württemberg (to W.K.), Germany, is gratefully acknowledged.

Conflict of interest

The authors declare no conflict of interest.

Keywords: epindolidione · redox non-innocence · ruthenium · spectroelectrochemistry · structure

[1] W. Beck, K. Sünkel, *Z. Anorg. Allg. Chem.* **2020**, *646*, 248–255.
[2] W. Kaim, G. K. Lahiri, *Coord. Chem. Rev.* **2019**, *393*, 1–8.
[3] W. Kaim, *Inorg. Chem.* **2011**, *50*, 9752–9765.
[4] E. E. Jaffe, H. Matrick, *J. Org. Chem.* **1968**, *33*, 4004–4010.
[5] A. O. F. Jones, C. Röthel, R. Lassnig, O. N. Bedoya-Martinez, P. Christian, I. Salzmann, B. Kunert, A. Winkler, R. Resel, *Cryst. Eng. Comm.* **2017**, *19*, 1902–1911.
[6] M. Klessinger, W. Lüttke, *Tetrahedron* **1963**, *19*, 315–335.

[7] C. Schmidt, W. Beck, *Z. Naturforsch. B* **1993**, *48*, 189 – 194.
[8] E. D. Głowacki, G. Romanazzi, C. Yumusak, H. Coskun, U. Monkawius, G. Voss, M. Burian, R. T. Lechner, N. Demitri, G. J. Redhammer, N. Sünger, G. P. Suranna, S. Sariciftci, *Adv. Funct. Mater.* **2015**, *25*, 776 – 787.
[9] C.-Y. Yang, K. Shi, T. Lei, J. Wang, X.-Y. Wang, F.-D. Zhuang, J.-Y. Wang, J. Pei, *ACS Appl. Mater. Interfaces* **2016**, *8*, 3714 – 3718.
[10] R. Lassnig, B. Striedinger, A. O. F. Jones, B. Schwerwitzl, A. Fian, E. D. Głowacki, B. Stadlober, A. Winkler, *Synth. Met.* **2016**, *218*, 64 – 74.
[11] E. Miglbauer, N. Demitri, M. Himmelsbach, U. Monkowius, N. S. Sariciftci, E. D. Głowacki, K. T. Oppelt, *ChemistrySelect* **2016**, *1*, 6349 – 6355.
[12] C. Liewald, S. Strohmair, H. Hecht, E. Głowacki, *Organic Electronics* **2018**, *60*, 51 – 56.
[13] M. Irimia-Vladu, Y. Kanbur, F. Camaioni, M. E. Coppola, C. Yumusak, C. Vlad Irimia, A. Vlad, A. Operamolla, G. M. Farinola, G. P. Suranna, N. González-Benitez, M. C. Molina, L. F. Bautista, H. Langhals, B. Stadlober, E. D. Głowacki, N. S. Sariciftci, *Chem. Mater.* **2019**, *31*, 6315 – 6346.
[14] W. Kaim, J. Fiedler, *Chem. Soc. Rev.* **2009**, *38*, 3373 – 3382.
[15] a) S. Herrero, M. A. Uson, *J. Chem. Educ.* **1995**, *72*, 1065-1066; b) F. F. Khan, J. Klein, J. L. Priego, B. Sarkar, R. Jiménez-Aparicio, G. K. Lahiri, *Inorg. Chem.* **2018**, *57*, 12800 – 12810.
[16] A. Das, P. Ghosh, S. Plebst, B. Schwederski, S. M. Mobin, W. Kaim, G. K. Lahiri, *Inorg. Chem.* **2015**, *54*, 3376 – 3386.
[17] S. Panda, S. K. Bera, G. K. Lahiri, *Polyhedron* **2019**, *172*, 45 – 57.
[18] W. Kaim, A. Klein, M. Glöckle, *Acc. Chem. Res.* **2000**, *33*, 755 – 763.
[19] W. Kaim, G. K. Lahiri, *Angew. Chem. Int. Ed.* **2007**, *46*, 1778 – 1796; *Angew. Chem.* **2007**, *119*, 1808 – 1828.
[20] W. Kaim, S. Ernst, V. Kasack, *J. Am. Chem. Soc.* **1990**, *112*, 173 – 178.
[21] W. Kaim, *Coord. Chem. Rev.* **1987**, *76*, 187 – 235.
[22] a) V. Kasack, W. Kaim, H. Binder, J. Jordanov, E. Roth, *Inorg. Chem.* **1995**, *34*, 1924 – 1933; b) S. Ernst, P. Hänel, J. Jordanov, W. Kaim, V. Kasack, E. Roth, *J. Am. Chem. Soc.* **1989**, *111*, 1733 – 1738.
[23] W. Kaim in *Electron Transfer in Chemistry, Vol. 2* (Ed.: V. Balzani), Wiley-VCH, Weinheim, **2001**, pp. 976 – 1002.
[24] M. Krejčik, M. Danek, F. Hartl, *J. Electroanal. Chem. Interfacial Electrochem.* **1991**, *317*, 179 – 187.
[25] a) P. Mondal, M. Chatterjee, A. Paretzki, K. Beyer, W. Kaim, G. K. Lahiri, *Inorg. Chem.* **2016**, *55*, 3105 – 3116; b) M. Chatterjee, P. Mondal, K. Beyer, A. Paretzki, W. Kaim, G. K. Lahiri, *Dalton Trans.* **2017**, *46*, 5091 – 5102.
[26] W. Kaim, *Coord. Chem. Rev.* **2011**, *255*, 2503 – 2513.
[27] S. Panda, M. A. Ansari, A. Mandal, G. K. Lahiri, *Chem. Asian J.* **2019**, *14*, 4631 – 4640.
[28] a) R. A. Krause, *Inorg. Chim. Acta* **1978**, *31*, 241 – 242; b) S. Goswami, A. R. Chakravarty, A. Chakravorty, *Inorg. Chem.* **1983**, *22*, 602 – 609.
[29] a) G. M. Sheldrick, *Acta Crystallogr. Sect. A* **2008**, *64*, 112 – 122; b) *Program for Crystal Structure Solution and Refinement*, University of Göttingen, Göttingen, Germany, **1997**; c) G. M. Sheldrick, *Acta Crystallogr. Sect. C* **2015**, *71*, 3 – 8.
[30] P. van der Sluis, A. L. Spek, *Acta Crystallogr. Sect. A* **1990**, *46*, 194 – 201.
[31] C. Lee, W. Yang, R. G. Parr, *Phys. Rev. B.* **1988**, *37*, 785 – 789.
[32] a) D. Andrae, U. Haeussermann, M. Dolg, H. Stoll, H. Preuss, *Theor. Chim. Acta* **1990**, *77*, 123 – 141; b) P. Fuentealba, H. Preuss, H. Stoll, L. von Szentpaly, *Chem. Phys. Lett.* **1982**, *89*, 418 – 422.
[33] Gaussian 09, Revision A.02, M. J. Frisch, G. W. Trucks, H. B. Schlegel, G. E. Scuseria, M. A. Robb, J. R. Cheeseman, G. Scalmani, V. Barone, B. Mennucci, G. A. Petersson, H. Nakatsuji, M. Caricato, X. Li, H. P. Hratchian, A. F. Izmaylov, J. Bloino, G. Zheng, J. L. Sonnenberg, M. Hada, M. Ehara, K. Toyota, R. Fukuda, J. Hasegawa, M. Ishida, T. Nakajima, Y. Honda, O. Kitao, H. Nakai, T. Vreven, J. A. Montgomery, Jr., J. E. Peralta, F. Ogliaro, M. Bearpark, J. J. Heyd, E. Brothers, K. N. Kudin, V. N. Staroverov, R. Kobayashi, J. Normand, K. Raghavachari, A. Rendell, J. C. Burant, S. S. Iyengar, J. Tomasi, M. Cossi, N. Rega, J. M. Millam, M. Klene, J. E. Knox, J. B. Cross, V. Bakken, C. Adamo, J. Jaramillo, R. Gomperts, R. E. Stratmann, O. Yazyev, A. J. Austin, R. Cammi, C. Pomelli, J. W. Ochterski, R. L. Martin, K. Morokuma, V. G. Zakrzewski, G. A. Voth, P. Salvador, J. J. Dannenberg, S. Dapprich, A. D. Daniels, O. Farkas, J. B. Foresman, J. V. Ortiz, J. Cioslowski, D. J. Fox, Gaussian, Inc., Wallingford CT, **2009**.
[34] a) R. Bauernschmitt, R. Ahlrichs, *Chem. Phys. Lett.* **1996**, *256*, 454 – 464; b) R. E. Stratmann, G. E. Scuseria, M. J. Frisch, *J. Chem. Phys.* **1998**, *109*, 8218 – 8225; c) M. E. Casida, C. Jamorski, K. C. Casida, D. R. Salahub, *J. Chem. Phys.* **1998**, *108*, 4439 – 4450.
[35] a) V. Barone, M. Cossi, *J. Phys. Chem. A* **1998**, *102*, 1995 – 2001; b) M. Cossi, V. Barone, *J. Chem. Phys.* **2001**, *115*, 4708 – 4718; c) M. Cossi, N. Rega, G. Scalmani, V. Barone, *J. Comput. Chem.* **2003**, *24*, 669 – 681.
[36] S. Leonid, *Chemissian 1.7*; **2005 – 2010**. Available at: http://www.chemissian.com.
[37] D. A. Zhurko, G. A. Zhurko, *ChemCraft 1.5*, Plimus, San Diego, CA. Available at: http://www.chemcraftprog.com.

Manuscript received: October 28, 2020
Revised manuscript received: December 9, 2020
Accepted manuscript online: January 18, 2021
Version of record online: February 26, 2021

